Published in final edited form as:
Nat Neurosci. 2008 January ; 11(1): 80–87. doi:10.1038/nn2030.

Activity-dependent gating of lateral inhibition in the mouse olfactory bulb

Armen C Arevian[1,2], **Vikrant Kapoor**[2,3], and **Nathaniel N Urban**[1,2,3]

[1]Center for Neuroscience, University of Pittsburgh, A210 Langley Hall, Pittsburgh, Pennsylvania 15260, USA

[2]Center for the Neural Basis of Cognition, 4400 Fifth Avenue, Pittsburgh, Pennsylvania 15213, USA

[3]Department of Biology, Carnegie Mellon University, 4400 Fifth Avenue, Pittsburgh, Pennsylvania 15213, USA

Abstract

Lateral inhibition is a circuit motif found throughout the nervous system that often generates contrast enhancement and center-surround receptive fields. We investigated the functional properties of the circuits mediating lateral inhibition between olfactory bulb principal neurons (mitral cells) *in vitro*. We found that the lateral inhibition received by mitral cells is gated by postsynaptic firing, such that a minimum threshold of postsynaptic activity is required before effective lateral inhibition is recruited. This dynamic regulation allows the strength of lateral inhibition to be enhanced between cells with correlated activity. Simulations show that this regulation of lateral inhibition causes decorrelation of mitral cell activity that is evoked by similar stimuli, even when stimuli have no clear spatial structure. These results show that this previously unknown mechanism for specifying lateral inhibitory connections allows functional inhibitory connectivity to be dynamically remapped to relevant populations of neurons.

Lateral inhibitory circuits are known to enhance contrast, facilitate discrimination of similar stimuli and mediate competitive interactions between active neurons[1,2]. These properties are the results of reductions in the degree to which input-driven activity is correlated across neurons responding to stimuli[3]. However, for lateral inhibition to function effectively in this manner, inhibition must be stronger between cells that are activated by similar stimuli (that is, between cells having correlated activity)[4]. When information is represented topographically, similar stimuli activate nearby neurons, so local inhibitory interactions are an effective means for contrast enhancement. This arrangement ensures that cells with correlated activity have strong inhibitory connectivity[5]. However, there are alternative strategies for specifying effective lateral inhibitory connectivity. For example, neurons with similar receptive fields can be connected specifically, independent of their proximity[6]. In this study, we investigate a third possibility, in which the strength of lateral inhibition is dynamically enhanced between neurons with correlated activity.

On the basis of the known properties of olfactory bulb circuits, we hypothesized that such a dynamic specification of inhibitory connectivity may be possible and functionally useful in the

Correspondence should be addressed to N.N.U. (E-mail: nurban@cmu.edu).

Note: Supplementary information is available on the Nature Neuroscience website.

Author Contributions: A.A. and N.U. designed all experiments (including computational) except for those in Figure 5, which were designed by V.K. and N.U. A.A. conducted and analyzed all experiments except for those in Figure 5, which were conducted and analyzed by V.K. A.A. and N.U. wrote the manuscript.

olfactory bulb[7]. At the level of olfactory receptor–neuron input to the olfactory bulb, stimuli are thought to be represented combinatorially with discontinuous topography[8–11]. Connectivity between mitral cells (the principal neurons of the olfactory bulb) lacks obvious patterning[12,13]. Single-molecule odorants activate many glomeruli that are distributed widely across the surface of the bulb. Unrelated odors can activate glomeruli in nearby areas and structural similarity of odorant molecules is often only weakly correlated with the relative position of the activated glomeruli[8,10,14,15].

Lateral inhibition in the olfactory bulb is mediated largely by reciprocal dendrodendritic synaptic connections between mitral-cell lateral dendrites and the dendrites of inhibitory granule cells[16,17]. Mitral-cell dendritic trees are radially symmetric, spanning an area up to 2 mm in diameter, connecting (disynaptically via the granule cells) a single mitral cell with as many as half of all the other mitral cells in the bulb[18,19]. These lateral dendrites release glutamate that depolarizes granule cell dendrites, which in turn release GABA back onto the presynaptic mitral cell (recurrent inhibition), as well as onto other mitral cells (lateral inhibition)[17]. The same population of granule cell– to–mitral cell synapses mediates both recurrent and lateral inhibition[20]. This suggests that when multiple mitral cells are active, recurrent and lateral inhibition will interact because multiple mitral cells will excite overlapping populations of granule cells (see Supplementary Figs. 1 and 2 online). Such an arrangement may allow mitral cells to regulate (via their own activity and the input they provide to granule cells) the effectiveness of the lateral inhibition that they receive. Specifically, we predicted that the output of weakly activated granule cells would be facilitated by the activity of a given mitral cell, enhancing the lateral inhibition that this cell receives, similar to what has been reported recently in cortical circuits[21]. In contrast, when granule cells are strongly active, additional input to these cells will not generate additional output.

The functional properties of inhibitory circuitry in the olfactory bulb are not well understood and the role of this circuitry in stimulus coding is controversial[22]. Here we show that the efficacy of lateral inhibition from an active mitral cell is enhanced when the postsynaptic mitral cell is also firing (that is, when the mitral cells show correlated activity). We used simulations to demonstrate that this activity-dependent enhancement of inhibition allows functional properties of lateral inhibition to be implemented even when inputs are nontopographic and connectivity is spatially uniform.

Results

To investigate the regulation of lateral inhibition by the activity of postsynaptic mitral cells, we recorded from these cells in slices of mouse main olfactory bulb while evoking lateral inhibitory postsynaptic potentials (IPSPs) via extracellular stimulation of nearby mitral cells. Mitral cells were activated by stimulation in the glomerular layer (40 pulses at 100 Hz, ~200 μm from the recorded mitral cell; Fig. 1a). Care was taken not to stimulate the glomerulus of the recorded mitral cell, which invariably resulted in excitatory postsynaptic potentials (EPSPs). The IPSPs evoked had a maximum amplitude of <2 mV and typically showed synaptic depression (Fig. 1b)[23]. By injecting current steps of various amplitudes (400 ms, 0–1,200 pA) into the mitral cell, we determined the relationship between firing frequency and injected current (*F-I* curve) of the postsynaptic mitral cell. *F-I* curves (Fig. 1c,d) obtained by current injection alone were compared with curves that were generated while eliciting IPSPs by extracellular stimulation. These data show that extracellular stimulation had no effect on mitral cell firing rate when the cells fired at low-to-moderate frequencies (0–25 Hz) or at very high frequencies (>65 Hz). Mitral cell firing was reduced by lateral inhibition specifically when cells were firing between 25 and 65 Hz (Fig. 1e; 24 ± 4.1% (blue line) and 7 ± 1.25 Hz (red line) average peak reduction between 25 and 65 Hz, $n = 7$, $P < 0.05$). Thus, we concluded that

the efficacy of lateral inhibition is enhanced in a frequency-specific manner when mitral cells are firing at intermediate rates.

We next tested whether gating of inhibition by postsynaptic activity could be seen in the most basic unit of lateral inhibition: the circuit consisting of two mitral cells and their associated granule cells. We made simultaneous recordings from pairs of mitral cells (Fig. 2a,b) and generated *F-I* curves in one mitral cell (chosen randomly and referred to as the postsynaptic cell) while stimulating the second mitral cell (referred to as the presynaptic cell) at a high, fixed rate (between 60 and 100 Hz) on alternate sweeps. Similar to the experiment above, the activity of a single presynaptic mitral cell reduced the firing rate of the postsynaptic mitral cell, but only when that cell was firing in a particular range of frequencies (Fig. 2c,d). We observed a reduction in postsynaptic firing rate in 15 out of the 29 pairs tested; in all cases in which inhibition was observed, its effectiveness was reduced or absent at very low and very high firing rates. The remaining pairs did not show any change in firing rate between the two conditions tested and may represent mitral cell pairs that form either no or only very weak synapses with overlapping populations of granule cells[12]. In these paired recordings, mitral cells were significantly inhibited when their postsynaptic firing rates were between 35 and 110 Hz (n = 15 pairs, $P < 0.05$, 18 ± 2.7% (blue line) and 8.7 ± 1.4 Hz (red line) average peak reduction in firing rate; Fig. 2e). The magnitude of inhibition was largest at 81 Hz when averaged across all of the mitral cell pairs (Fig. 2e, red line). We determined the range of firing rates over which inhibition was observed for the population of 15 mitral cell pairs showing a reduction in postsynaptic firing rate (summarized in Fig. 3a). On average, mitral cells were inhibited over a 32 ± 7–Hz range of postsynaptic firing rates. Notably, this inhibition occurred in many cases, despite there being no observation of any obvious IPSPs resulting from presynaptic activity alone (for example, Fig. 2b, top panel). This suggests the cooperative activation of the inhibitory granule cells by multiple mitral cells is critical to this phenomenon (see Discussion). We confirmed that the inhibition that we observed was at least in part due to granule cells, as mitral cells that had their apical dendrites cut proximal to the tuft (as in Fig. 2a) still showed activity-dependent gating of lateral inhibition, even though these cells would receive no inhibition from periglomerular cells.

We next wanted to determine how mitral cell spike-timing was altered by lateral inhibition, given that results indicate the importance of spike timing and inhibition in olfactory processing in the bulb[3,24–26]. To accomplish this, we computed the difference in the time-dependent firing rate from our paired recordings between trials with and without presynaptic mitral-cell activity. Spike trains from the postsynaptic cell were smoothed with a Gaussian (s.d. of 45 ms), the smoothed firing rates for these two conditions were subtracted and these differences were averaged across all 15 pairs (Fig. 3b). This analysis allowed us to determine when, during the 400-ms period of activity, lateral inhibition most effectively reduced firing. We found that at low postsynaptic firing rates, inhibition was weak and unreliable. At higher firing rates (~60 Hz), the largest reduction in firing rate was observed during the last 40 ms of the 400-ms firing period. Further increases in postsynaptic activity resulted in inhibition that began earlier and had a larger peak magnitude (−40 ± 5% instantaneous reduction of postsynaptic firing rate at 167 ± 32 ms after stimulus onset at 67 ± 9 Hz.) The large magnitude inhibition observed at high postsynaptic firing rates had a maximum duration of approximately 300 ms. This is consistent with the observation that granule cell–mediated lateral inhibition undergoes synaptic depression during repetitive stimulation[23,27], and indicates that the strength of lateral inhibition between mitral cells not only depends on the instantaneous levels of pre- and postsynaptic activity, but also on the recent history of activity.

As an independent measure of lateral inhibition we also examined the magnitude of recurrent IPSPs recorded in the postsynaptic mitral cell with and without activity of the presynaptic cell. We quantified recurrent inhibition by measuring the hyperpolarization following a 400-ms

train of action potentials of a given frequency[28]. This hyperpolarization was 31 ± 4.4% larger on trials in which the presynaptic mitral cell was firing, even when controlling for the firing rate of the postsynaptic cell (from −3.4 ± 0.7 to −4.6 ± 0.6 mV for 22 ± 3.4–Hz activity, $P < 0.01$; Fig. 3c). These data demonstrate that stimulation of a single presynaptic mitral cell is sufficient to enhance recurrent inhibition. Because the hyperpolarization following trains of action potentials results from a combination of synaptic and intrinsic conductances[28,29], the increased hyperpolarization that we observed may underestimate the actual increase in synaptic inhibition[28]. We also examined whether granule cell–mediated inhibition was enhanced by temporal precision of mitral cell spiking (Fig. 3d). To test this, we varied the timing of spiking in a single mitral cell to examine whether groups of action potentials at short intervals recruited additional inhibition. We found that changing the action potential train from one with uniform intervals (8 spikes at 40 ms) to one in which spikes were clustered (4 pairs of spikes at 40 ms) had no effect on the magnitude of granule cell–mediated recurrent inhibition ($P > 0.8$, $n = 5$). The lack of sensitivity to temporal coincidence of input in granule cells is consistent with the observation that they respond at long latencies[26] and are best activated by prolonged inputs[30] (see Discussion).

We hypothesized that the gating of lateral inhibition by coincident activity in mitral cell pairs is a result of granule cells receiving common input from the mitral cells, and that coincident activity of these mitral cells recruits additional granule cells, which then contribute additional lateral inhibition[7] (Supplementary Figs. 1 and 2). This hypothesis predicts that increasing the firing rate of the presynaptic mitral cell should decrease the requirement for high-frequency firing in the second mitral cell, and thus shift the range of postsynaptic firing rates over which activity-dependent gating of lateral inhibition occurs. To test this prediction, we generated *F-I* curves for a postsynaptic mitral cell while stimulating the presynaptic cell at 50 or 100 Hz, and compared this with the control condition of no presynaptic stimulation. As predicted, we observed that increasing the presynaptic firing rate from 50 to 100 Hz shifted the range of firing rates over which the postsynaptic mitral cell was inhibited to lower frequencies (Fig. 3e–g, $n = 6$, $P < 0.05$). Furthermore, there was a significant increase in the magnitude of lateral inhibition, measured as the fractional change in activity (Fig. 3h $n = 6$, $P < 0.05$), although the absolute change in firing rate was not significantly affected ($P = 0.69$, $n = 6$).

Our proposed mechanism would predict that the direct activation of granule cells should generate lateral inhibition that is less dependent on simultaneous activation of postsynaptic mitral cells. Therefore, we stimulated granule cells directly by placing extracellular stimulation electrodes in the granule cell layer while recording from a single mitral cell (Fig. 4). As predicted, direct activation of granule cells inhibited mitral cell firing throughout much of the mitral cell *F-I* curve, with the inhibition saturating at very high firing rates ($n = 9$, compare Figs. 1e and 4e, blue lines). To investigate the role of the postsynaptic mitral cell, we blocked ionotropic glutamate receptors (with 50 μM APV and 10 μM CNQX), which blocked the ability of the recorded mitral cell to contribute to the inhibition that it receives. This blockade had minimal effect on inhibition evoked by granule-cell stimulation when mitral cells were firing at low and high firing rates, but substantially reduced the inhibition observed at intermediate mitral-cell firing rates (firing rate in APV and CNQX during ECS was 59% higher at 25 Hz and significantly higher only from 12–44 Hz, $n = 4$, $P < 0.05$; Fig. 4e, green line). This result indicates that the release of glutamate from postsynaptic mitral cells causes enhanced granule cell–mediated lateral inhibition specifically in this intermediate range of firing rates, consistent with our prediction.

We examined the recruitment of granule cells by combined mitral cell inputs in more detail by imaging activity, in the form of calcium transients, in populations of granule cells following extracellular stimulation of single glomeruli. Previously, we have shown that granule cell calcium transients observed under these conditions are correlated with granule cell spiking[26].

Extracellular stimulation of nearby glomeruli activated distinct populations of mitral cells and partially overlapping populations of granule cells, as reported previously[26] (about 29 ± 4% overlap, $n = 5$ slices, 120 granule cells activated by stimulation of at least one of the two glomeruli; Fig. 5a, top left). This shows that mitral cells in different glomeruli connect to common populations of granule cells. Simultaneous stimulation of the two glomeruli resulted in the recruitment of 50 ± 16% more granule cells ($P < 0.05$, $n = 5$ slices) than the total that were activated by the stimulation of either of the two glomeruli singly (182 cells activated by simultaneous stimulation of two glomeruli, $n = 5$ slices: Fig. 5a,b). These data show that when independent populations of mitral cells are stimulated, granule cells are activated in a cooperative fashion (Supplementary Fig. 1). This will allow the amplitude of lateral inhibition to increase nonlinearly as more mitral cells are recruited[21].

These physiological data suggest that the number of activated granule cells, and thus the strength of inhibition, is regulated dynamically by correlated mitral cell activity. Such a mechanism will allow lateral inhibition to be rapidly remapped across populations of activated mitral cells. The fractured manner in which odor-evoked patterns of activity are mapped onto the bulb[31] suggests that such a dynamic activity-dependent regulation of lateral inhibition may be required to enhance contrast and facilitate discrimination between patterns of odor-evoked mitral cell activity[4]. We used a model to investigate whether this mechanism can effectively enhance contrast between mitral cells with similar response profiles. The key features of this model were that the strength of lateral inhibition was maximal at intermediate levels of postsynaptic activity, as we observed in our experiments (compare Figs. 2d and 6a), and that the connectivity in the model was all-to-all, and thus had no spatial structure. Using this model, we tested whether such circuits would be sufficient to enhance contrast between similar stimuli and to decorrelate activity across populations of mitral cells responding to similar odors, similar to what has been observed *in vivo*[3]. The firing rate at which the strength of lateral inhibition was maximal was chosen to be approximately the mean activity in the network. Olfactory receptor–neuron activity was simulated by randomly assigning activity values to 60 points in a 25 × 25 array and convolving the map with a circular Gaussian function (s.d. of two pixels). After processing by activity-dependent lateral inhibition, the output of the network (analogous to mitral cell activity) showed increased contrast as compared with the initial input (Fig. 6b). In some examples, we tested whether spatial patterning was important by randomizing the positions of all pixels before running the simulation and then unrandomizing after the network had reached steady state (see Supplementary Fig. 3 online). This randomization had no effect on the processing of the model, as would be expected given the all-to-all connectivity in the model.

We next examined the effect of dynamic lateral inhibition on simulated patterns of olfactory receptor–neuron inputs with varying degrees of similarity. We generated 16 input maps with varying degrees of correlation (Fig. 6c, see Methods). If activity-dependent lateral inhibition functions to increase the discriminability of similar odors, we should observe a decrease in correlation between initially similar responses, similar to that observed *in vivo*[3]. As predicted, applying this activity-dependent lateral inhibition to each map decreased the correlation between initially similar patterns of simulated odor-evoked activity. This change was evident in the cross-correlation matrices (compare left and right panels in Fig. 6c) and by computing the average level of pair-wise correlations of input and output (Fig. 6d,e). Models in which the strength of inhibition was independent of postsynaptic activity did not generate substantial levels of decorrelation, even when the overall level of inhibition reduced activity to a greater degree (Fig. 6d,e). This observation held whether the inhibition was modeled as subtractive or divisive, indicating that the activity dependence of lateral inhibition is critical for mediating decorrelation in networks without spatial structure to their connections (average pair-wise correlation across all maps of 0.33: closed arrow, reduced to 0.11; open arrow, by activity-dependent lateral inhibition; Fig. 6d). To determine whether the residual inhibition at higher

firing rates that we sometimes observed in our experiments (Fig. 1c,d) affects the computational functions of the model, we tested the model with a substantial amount of residual inhibition (50% residual inhibition relative to peak inhibition; Fig. 6a, dotted line). Even with this substantial amount of residual inhibition, the model still showed robust decorrelation (Fig. 6e) [3,32,33]. One difference between our simulations and the data on time-dependent decorrelation is that we did not see examples of patterns of activity evoked by two different odors becoming increasingly correlated across time, as is seen in a subset of cells recorded experimentally[3]. This may be a result of the simplicity of our model, which does not include features such as excitatory coupling between mitral cells[27,34,35] or short-term plasticity of lateral inhibition[23] that may be important for these aspects of the described results. As a demonstration, we also tested this mechanism for specifying lateral inhibition on an image-processing application. When an image was given as the stimulus to a larger, but otherwise identical, network model, activity-dependent lateral inhibition resulted in substantial contrast enhancement even when applied to a version of the image in which pixel position was randomized (Fig. 6f and Supplementary Fig. 3). This independence of the operation on the spatial structure contained in the image represents a previously unknown method of enhancing contrast in images.

Discussion

We have explored the functional properties of the circuit mediating lateral inhibition in the olfactory bulb. This circuit consists of pre- and postsynaptic mitral cells reciprocally connected via dendrodendritic synapses with inhibitory granule cells. We have shown that activity of a postsynaptic mitral cell influences the effectiveness of the lateral inhibition that it receives and that this is a result of the integration of activity from multiple mitral cells by those granule cells that provide lateral inhibitory input (Supplementary Figs. 1 and 2). Moreover, using simulations, we show that such activity-dependent lateral inhibition generates contrast enhancement without spatially structured inputs or connections.

The key requirement for this phenomenon is that the activity of the postsynaptic mitral cell is able to influence the output of the inhibitory granule cell from which it receives input. In the olfactory bulb circuit, mitral cell–to–granule cell connections are almost 100% reciprocal, favoring such interactions[12]. The nature of this influence depends on the level of activity. At moderate levels of activity, correlated activity across mitral cells increases the strength of lateral inhibition as a result of cooperative activation of granule cells by the two mitral cells (Supplementary Fig. 2). That is, when mitral cells are firing at moderate rates, recurrent inhibition is weak and GABA release from granule cells is increased during coincident input from pre- and postsynaptic mitral cells. At high levels of postsynaptic activity, release from granule cells has been shown to saturate[27,28]. In this case, additional input to granule cells from the presynaptic mitral cell is ineffective at evoking additional inhibitory input (Supplementary Fig. 2). This gating of lateral inhibition by postsynaptic activity thus depends critically on nonlinear integration of multiple mitral-cell inputs by granule cells.

Granule cell activity is known to depend critically on several mechanisms that may mediate coincidence detection, including the NMDA receptor and inactivating potassium channels[29,34,36]. Spatial integration of excitatory input in the granule cell dendritic tree also could be important[37]. Furthermore, because granule cell–mediated recurrent and lateral inhibition saturate at higher firing rates[23,27,28], strongly active mitral cells ‘immunize’ themselves against lateral inhibition by activating a large fraction of the granule cells that provide them with inhibition. The firing rates required for this suppression of inhibition, although high, are observed *in vivo* in anaesthetized preparations[28,38]. This allows for information in cells firing at high rates to be preserved. These data demonstrate how strongly inhibition in the olfactory bulb is influenced by population activity, but also show that the firing of even a single mitral cell is sufficient to generate a significant reduction of firing rate in many other mitral cells.

Increasing the number of active mitral cells increases both the range and efficacy of lateral inhibition, as it activates granule cells to both sub- and superthreshold levels[26]. Together, these data provide a plausible implementation of the kind of connectivity that is required to achieve useful competitive interactions between active mitral cells. A similar sort of connectivity has also been proposed as the most effective for explaining *in vivo* physiological data from honeybee olfactory system[4].

How does activity-dependent lateral inhibition differ from conventional center-surround mechanisms of lateral inhibition? Activity-dependent lateral inhibition operates not on the spatial structure of the representation *per se*, but rather on the distribution of activity (that is, the histogram of firing rates). With long range inhibitory connectivity, as is seen between olfactory bulb mitral cells, activity-dependent lateral inhibition will change the distribution of activity across mitral cells. Mitral cells active at some intermediate range will have their activity reduced, with the amount of the reduction depending the cell's own activity and on the average activity level across the population. Functionally, this will increase the separation between those cells that are firing at the highest rates and those firing at intermediate or lower rates, resulting in a kind of contrast enhancement that does not depend on spatial features of the representation. Although results from our model indicate that input patterns are decorrelated in a manner that is independent of spatial patterning, this does not rule out a role for the broad groupings of olfactory receptor types that have been reported[39,40]. This broad grouping could function to ensure that mitral cells responding to related odors are located in regions that are linked by their lateral dendrites and associated granule cells.

Although our work has focused exclusively on the olfactory bulb, there are many brain areas (such as inferotemporal cortex and hippocampus) in which stimuli are not represented in obviously topographical ways[41,42]. Physiological data on the superlinear summation of inhibition in neocortical circuits[21] suggests that some features of activity-dependent lateral inhibition may be implemented in neocortical areas. Thus, this mechanism may provide a powerful computational algorithm for increasing discriminability between similar inputs that could be employed in other brain systems, particularly those in which stimulus representation is combinatorial and connectivity is widespread. These findings represent a previously unknown and general computational mechanism for increasing discriminability between similar inputs on the basis of the known physiology of inhibition in the bulb, where inhibitory output is dynamically gated in an activity-dependent manner.

Methods

Slice preparation and electrophysiological recordings

All procedures were carried out in accordance with protocols approved by the Institutional Animal Care and Use Committee of Carnegie Mellon University. Sagittal slices of mouse olfactory bulb were prepared and whole-cell recordings were obtained according to procedures described previously[27,28].

Calcium imaging

Loading and imaging of fura-2 was carried out as described previously[26]. Briefly, olfactory bulb slices were incubated in a chamber containing 500 μl of Ringer's solution with 3 μl of 0.01% Pluronic (Molecular Probes) and 5 μl of a 1 mM solution of fura-2 acetoxymethyl ester (Molecular Probes) in 100% DMSO solution. Slices were incubated in this solution at 37 °C for 60–90 min.

Slices were imaged under an upright microscope using either a 20×, 40× or 60× water immersion objective. Slices were visualized for successful loading using excitation

wavelengths of 360–400 nm and emission wavelengths of 480–520 nm. Experiments were carried out at 37 °C and Ringer's solution had $Mg2^{+}$ reduced to 0.2 mM to facilitate activation of granule cells[26]. A cooled back-illuminated frame transfer CCD camera (Micromax 512 BFT, Princeton Instruments) was used to capture sequences of images with exposure times of 25–50 ms per frame at 3 × 3 binning (final image size, 170 × 170 pixels). Images were acquired and stored using software written in Igor Pro (Wavemetrics), using drivers (SIDX) from Bruxton Scientific. Videos were analyzed by first calculating $\Delta F/F$ frame by frame for whole videos. Sets of ten videos were collected for each condition. To determine the population of active cells we took the minimum (fura decreases its fluorescence when binding calcium in our conditions) pixel value from this set often videos. By taking the minimum projection, we may overestimate the number of active cells (if some cells are active spontaneously) in proportion to the number of trials being considered. In our conditions, however, there was very little spontaneous activity of granule cells, and so we consider this method to provide a good estimate of the number of active cells even when the probability of a cell being active is ~ 30%, as previously reported for granule cells[27]. Paired *t*-test used for all *P* value calculations (except Fig. 3e–g, where a Wilcoxon rank-sum test was used).

Computational model

To investigate the computational properties of the physiologically observed activity-dependent gating of lateral inhibition in this study, we developed a continuous–firing rate network model in Matlab (Mathworks). This model consisted of a 25 × 25 array of simulated nonspiking neurons representing olfactory bulb mitral cells, with their average firing rate represented by a continuous variable, v (equation (1)). Each neuron received background noise and contained a leak current. Additionally, neurons received a time-dependent stimulus, $stim(t)$, representing input from olfactory receptor neurons. This stimulus had a constant, nonzero value only for the time period indicated by the black bar in Figure 6d. The stimulus value was calculated for each neuron by multiplying the conductance (g_s; 0 for $t <$ tstart; 1 for $t \geq$ tstart) with a constant value E_s. The value for E_s was generated by randomly assigning activity values to 60 points in a 25 × 25 array and convolving the map with a circular Gaussian (s.d. of two pixels). To remove any spatial patterning of the stimulus in the model, neurons showed all-to-all connectivity. Inhibition was determined using one of three methods, depending on the condition being tested. For activity-dependent inhibition (equation (2)), inhibition was calculated by the sum of network activity, $u(t)$, as well as by an exponential function relying on the postsynaptic neurons firing rate. This exponential function approximated the activity-dependent gating of lateral inhibition observed in our results (compare Figs. 2d and 6a). For subtractive inhibition, the exponential function representing activity dependence was removed (equation (3)). To simulate divisive inhibition, a fraction of the neurons own firing rate was used to calculate the amount of inhibition that it received (equation (4)). To approximate the delayed onset of inhibition in the bulb, the inhibition in the model was multiplied by a delay function, $delay(t)$.

$$\begin{aligned} \tau\frac{dv}{dt} &= \text{noise} + \text{stim}(t) - \text{leak} - \text{inh}(t) \\ \text{noise} &= g_n \cdot \text{rand} \\ \text{stim}(t) &= g_s(t) \cdot (E_s) \\ \text{leak} &= g_l \cdot (v(t) - E_l) \end{aligned} \tag{1}$$

$$\text{inh}_a(t) = g_{ia} \cdot u(t) \cdot \text{delay}(t) \cdot e^{\frac{-(v(t)-\text{peak})^2}{\sigma}} \tag{2}$$

$$\mathrm{inh}_s(t) = g_{is} \cdot u(t) \cdot \mathrm{delay}(t) \tag{3}$$

$$\begin{aligned} \mathrm{inh}_d(t) &= g_{id} \cdot v(t) \cdot \mathrm{delay}(t) \\ u(t) &= \sum_{n=1}^{N} v_n(t) \\ \mathrm{delay}(t) &= 1 + g_d \cdot \tanh(t - t_{\mathrm{offset}}) \end{aligned} \tag{4}$$

To determine whether activity-dependent lateral inhibition could decorrelate initially similar inputs, we generated 16 different input maps with varying correlation (representing odors of varying similarity) for each 25 × 25 array of neurons. The digital image used in Figure 6f was captured using a Sony DSC-P72 digital camera. The image was down-sampled to 300 × 427 pixels and imported to Matlab. This image was then used as the input map for the computational model.

Supplementary Material

Refer to Web version on PubMed Central for supplementary material.

Acknowledgments

Thanks to A.T. Schaefer and members of the Urban laboratory for helpful comments and discussion. This work was supported by the grants from the National Institute of Deafness and Other Communication Disorders (F30 DC008274, A.A.; R01 DC005798, N.U.) and by a fellowship from the National Science Foundation Integrative Graduate Education and Research Traineeship program (NSF DGE-9987588, A.A.).

References

1. Hirsch JA, Gilbert CD. Synaptic physiology of horizontal connections in the cat's visual cortex. J Neurosci 1991;11:1800–1809. [PubMed: 1675266]
2. Urban NN. Lateral inhibition in the olfactory bulb and in olfaction. Physiol Behav 2002;77:607–612. [PubMed: 12527007]
3. Friedrich RW, Laurent G. Dynamic optimization of odor representations by slow temporal patterning of mitral cell activity. Science 2001;291:889–894. [PubMed: 11157170]
4. Linster C, Sachse S, Galizia CG. Computational modeling suggests that response properties rather than spatial position determine connectivity between olfactory glomeruli. J Neurophysiol 2005;93:3410–3417. [PubMed: 15673548]
5. Kuffler SW. Discharge patterns and functional organization of mammalian retina. J Neurophysiol 1953;16:37–68. [PubMed: 13035466]
6. Bosking WH, Zhang Y, Schofield B, Fitzpatrick D. Orientation selectivity and the arrangement of horizontal connections in tree shrew striate cortex. J Neurosci 1997;17:2112–2127. [PubMed: 9045738]
7. Jahr CE, Nicoll RA. An intracellular analysis of dendrodendritic inhibition in the turtle *in vitro* olfactory bulb. J Physiol (Lond) 1982;326:213–234. [PubMed: 7108788]
8. Uchida N, Takahashi YK, Tanifuji M, Mori K. Odor maps in the mammalian olfactory bulb: domain organization and odorant structural features. Nat Neurosci 2000;3:1035–1043. [PubMed: 11017177]
9. Takahashi YK, Kurosaki M, Hirono S, Mori K. Topographic representation of odorant molecular features in the rat olfactory bulb. J Neurophysiol 2004;92:2413–2427. [PubMed: 15152015]
10. Friedrich RW, Korsching SI. Combinatorial and chemotopic odorant coding in the zebrafish olfactory bulb visualized by optical imaging. Neuron 1997;18:737–752. [PubMed: 9182799]
11. Malnic B, Hirono J, Sato T, Buck LB. Combinatorial receptor codes for odors. Cell 1999;96:713–723. [PubMed: 10089886]

12. Egger V, Urban NN. Dynamic connectivity in the mitral cell-granule cell microcircuit. Semin Cell Dev Biol 2006;17:424–432. [PubMed: 16889994]
13. Willhite DC, et al. Viral tracing identifies distributed columnar organization in the olfactory bulb. Proc Natl Acad Sci USA 2006;103:12592–12597. [PubMed: 16895993]
14. Rubin BD, Katz LC. Optical imaging of odorant representations in the mammalian olfactory bulb. Neuron 1999;23:499–511. [PubMed: 10433262]
15. Meister M, Bonhoeffer T. Tuning and topography in an odor map on the rat olfactory bulb. J Neurosci 2001;21:1351–1360. [PubMed: 11160406]
16. Shepherd, GM.; Greer, CA. Olfactory bulb. In: Shepherd, GM., editor. The Synaptic Organization of the Brain. Oxford University Press; New York: 2004.
17. Schoppa NE, Urban NN. Dendritic processing within olfactory bulb circuits. Trends Neurosci 2003;26:501–506. [PubMed: 12948662]
18. Orona E, Rainer EC, Scott JW. Dendritic and axonal organization of mitral and tufted cells in the rat olfactory bulb. J Comp Neurol 1984;226:346–356. [PubMed: 6747027]
19. Mori K, Kishi K, Ojima H. Distribution of dendrites of mitral, displaced mitral, tufted and granule cells in the rabbit olfactory bulb. J Comp Neurol 1983;219:339–355. [PubMed: 6619342]
20. Price JL, Powell TP. The synaptology of the granule cells of the olfactory bulb. J Cell Sci 1970;7:125–155. [PubMed: 5476853]
21. Kapfer C, Glickfeld LL, Atallah BV, Scanziani M. Supralinear increase of recurrent inhibition during sparse activity in the somatosensory cortex. Nat Neurosci 2007;10:743–753. [PubMed: 17515899]
22. Laurent G. A systems perspective on early olfactory coding. Science 1999;286:723–728. [PubMed: 10531051]
23. Dietz SB, Murthy VN. Contrasting short-term plasticity at two sides of the mitral-granule reciprocal synapse in the mammalian olfactory bulb. J Physiol (Lond) 2005;569:475–488. [PubMed: 16166156]
24. Abraham NM, et al. Maintaining accuracy at the expense of speed: stimulus similarity defines odor discrimination time in mice. Neuron 2004;44:865–876. [PubMed: 15572116]
25. Uchida N, Mainen ZF. Speed and accuracy of olfactory discrimination in the rat. Nat Neurosci 2003;6:1224–1229. [PubMed: 14566341]
26. Kapoor V, Urban NN. Glomerulus-specific, long-latency activity in the olfactory bulb granule cell network. J Neurosci 2006;26:11709–11719. [PubMed: 17093092]
27. Urban NN, Sakmann B. Reciprocal intraglomerular excitation and intra- and interglomerular lateral inhibition between mouse olfactory bulb mitral cells. J Physiol (Lond) 2002;542:355–367. [PubMed: 12122137]
28. Margrie TW, Sakmann B, Urban NN. Action potential propagation in mitral cell lateral dendrites is decremental and controls recurrent and lateral inhibition in the mammalian olfactory bulb. Proc Natl Acad Sci USA 2001;98:319–324. [PubMed: 11120888]
29. Isaacson JS, Strowbridge BW. Olfactory reciprocal synapses: dendritic signaling in the CNS. Neuron 1998;20:749–761. [PubMed: 9581766]
30. Schoppa NE, Westbrook GL. Regulation of synaptic timing in the olfactory bulb by an A-type potassium current. Nat Neurosci 1999;2:1106–1113. [PubMed: 10570488]
31. Friedrich RW, Stopfer M. Recent dynamics in olfactory population coding. Curr Opin Neurobiol 2001;11:468–474. [PubMed: 11502394]
32. Wilson RI, Turner GC, Laurent G. Transformation of olfactory representations in the *Drosophila* antennal lobe. Science 2004;303:366–370. [PubMed: 14684826]
33. Stopfer M, Jayaraman V, Laurent G. Intensity versus identity coding in an olfactory system. Neuron 2003;39:991–1004. [PubMed: 12971898]
34. Schoppa NE, Westbrook GL. AMPA autoreceptors drive correlated spiking in olfactory bulb glomeruli. Nat Neurosci 2002;5:1194–1202. [PubMed: 12379859]
35. Carlson GC, Shipley MT, Keller A. Long-lasting depolarizations in mitral cells of the rat olfactory bulb. J Neurosci 2000;20:2011–2021. [PubMed: 10684902]
36. Schoppa NE, Kinzie JM, Sahara Y, Segerson TP, Westbrook GL. Dendrodendritic inhibition in the olfactory bulb is driven by NMDA receptors. J Neurosci 1998;18:6790–6802. [PubMed: 9712650]

37. Egger V, Svoboda K, Mainen ZF. Dendrodendritic synaptic signals in olfactory bulb granule cells: local spine boost and global low-threshold spike. J Neurosci 2005;25:3521–3530. [PubMed: 15814782]

38. Egana JI, Aylwin ML, Maldonado PE. Odor response properties of neighboring mitral/tufted cells in the rat olfactory bulb. Neuroscience 2005;134:1069–1080. [PubMed: 15994017]

39. Mori K, Takahashi YK, Igarashi KM, Yamaguchi M. Maps of odorant molecular features in the mammalian olfactory bulb. Physiol Rev 2006;86:409–433. [PubMed: 16601265]

40. Johnson BA, Farahbod H, Xu Z, Saber S, Leon M. Local and global chemotopic organization: general features of the glomerular representations of aliphatic odorants differing in carbon number. J Comp Neurol 2004;480:234–249. [PubMed: 15514935]

41. Leutgeb S, Leutgeb JK, Moser MB, Moser EI. Place cells, spatial maps and the population code for memory. Curr Opin Neurobiol 2005;15:738–746. [PubMed: 16263261]

42. Wang Y, Fujita I, Murayama Y. Neuronal mechanisms of selectivity for object features revealed by blocking inhibition in inferotemporal cortex. Nat Neurosci 2000;3:807–813. [PubMed: 10903574]

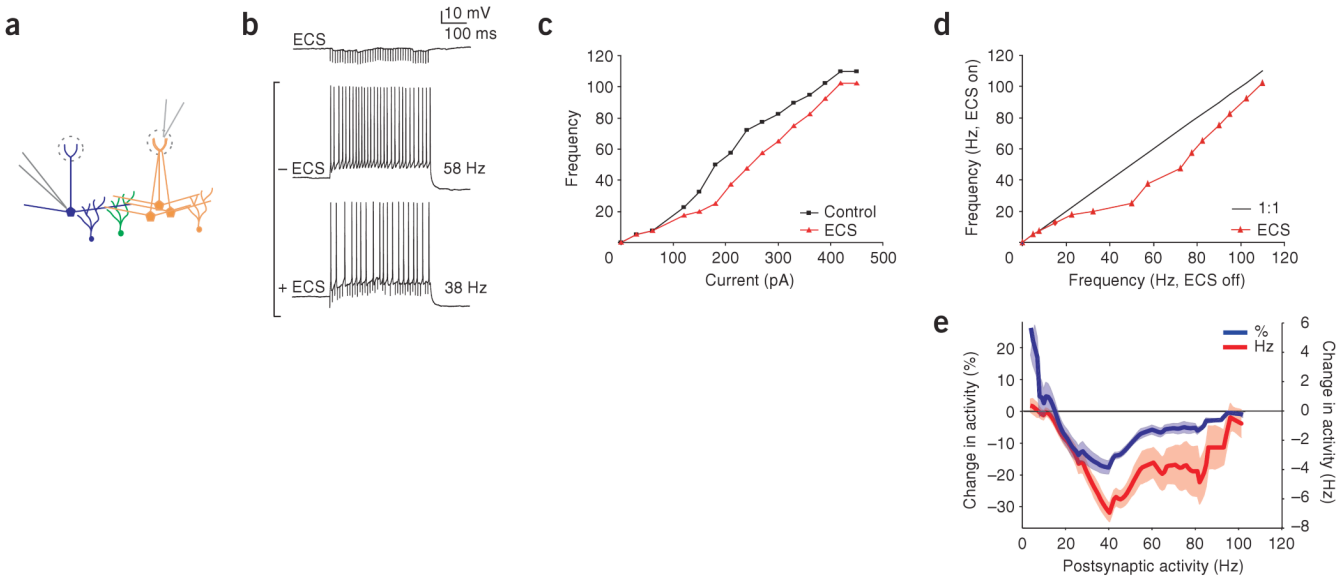

Figure 1.

Activity-dependent gating of lateral inhibition. (**a**) Schematic of experimental configuration. Whole-cell recording of a single mitral cell (blue cell, postsynaptic cell) during application of extracellular stimulation (ECS) in the glomerular layer, activating a population of presynaptic mitral cells (orange cells). Mitral cells were disynaptically connected via the shared population of granule cells (green cells). (**b**) ECS evoked IPSPs in the recorded mitral cell and resulted in inhibition of firing rate for a given current step. The control firing rate (58 Hz) was reduced (to 38 Hz) by ECS. (**c,d**) Effectiveness of ECS in reducing mitral cell firing rate is shown by plotting *F-I* curves (red line with ECS and black line without ECS, **c**) and by plotting frequency with and without ECS for the same current steps (**d**). (**e**) Percentage change (blue line), as well as absolute change, in activity (red line) as a function of firing rate averaged across recordings. Shaded areas for this and subsequent figures indicate s.e.m.

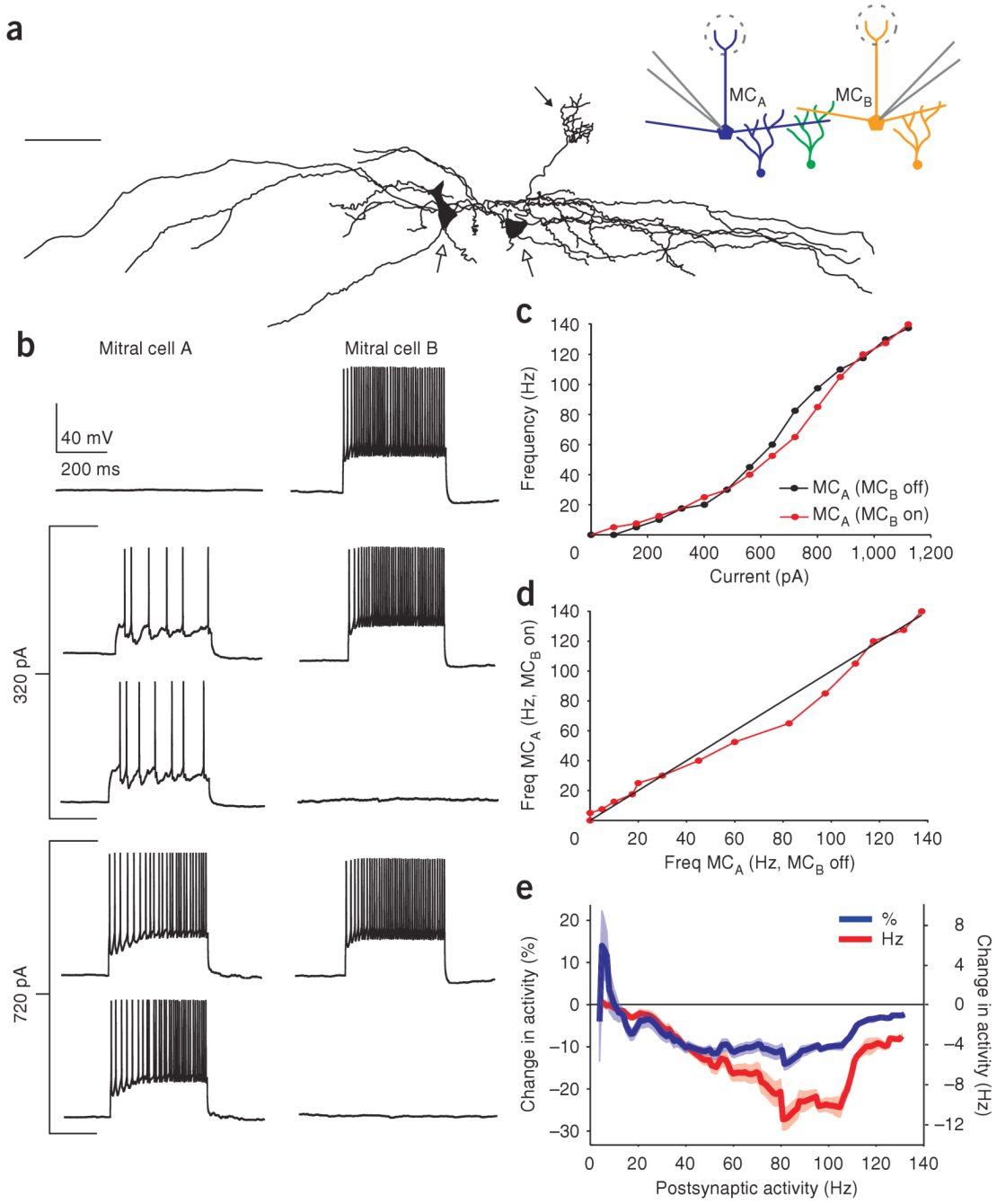

Figure 2.

Activity-dependent gating of lateral inhibition in mitral cell pairs. (**a**) Tracings from a biocytin-filled mitral-cell pair (scale bar, 75 μm). Open arrows indicate cell bodies, filled arrow indicates tuft of one mitral cell; the other cell had a cut primary dendrite. Inset, schematic of experiment. Whole-cell recording from pairs of mitral cells disynaptically connected via the shared population of granule cells are shown in green. (**b**) Activation of a single presynaptic mitral cell (mitral cell B, MC_B) did not result in IPSPs in the postsynaptic cell (mitral cell A, MC_A). Similarly, MC_B was ineffective at inhibiting MC_A when MC_A was firing at 32 Hz. However, at 85 Hz, MC_B was able to reduce the firing rate of MC_A to 65 Hz, representing a 24% reduction. (**c**) This activity-dependent inhibition is illustrated by comparing the *F-I* curves for the control

condition (MC_B off, red line) to the case when MC_B is activated (MC_B on, black line). (**d**) Firing rate of MC_A, plotted with respect to the two conditions tested, showing a selective reduction in the firing rate of MC_A only between 45 and 110 Hz. (**e**) Percentage (blue line) and absolute change in activity (red line) as a function of firing rate, averaged across paired recordings.

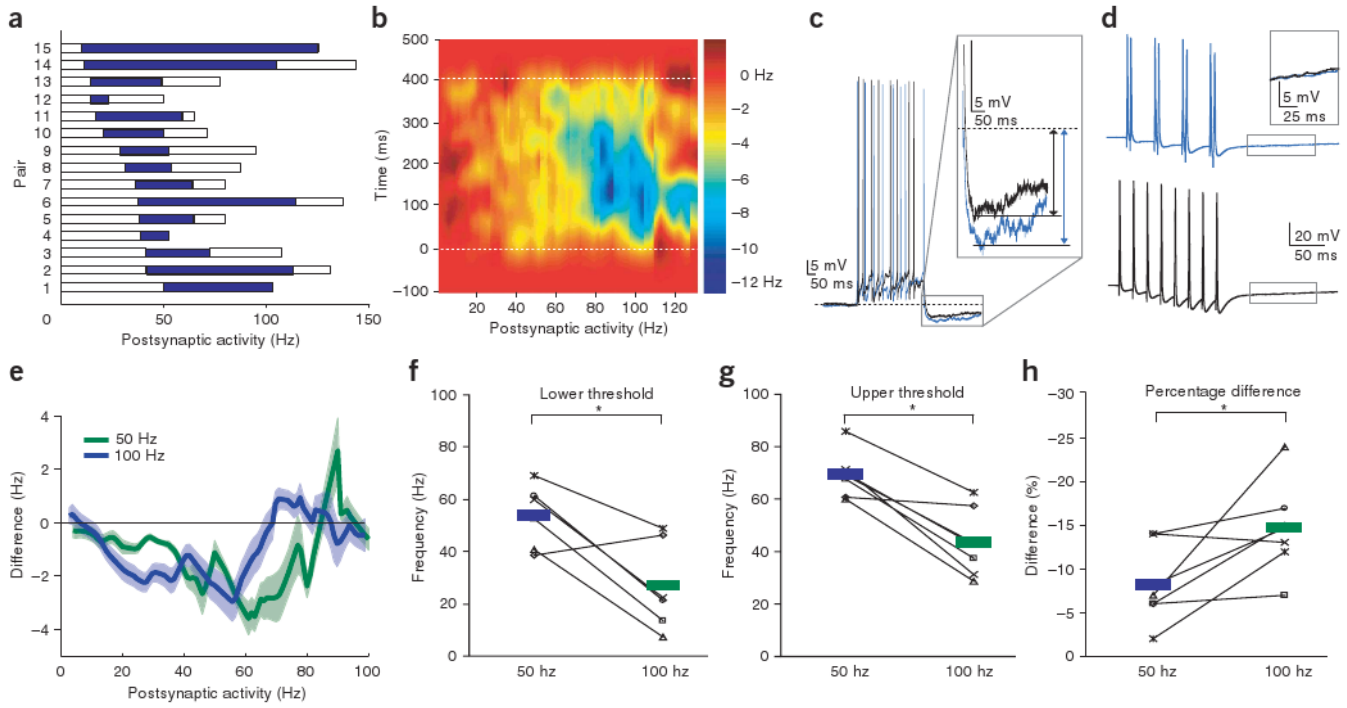

Figure 3.

Summary results of activity-dependent lateral inhibition. (**a**) Data from 15 mitral cell pairs showing lateral inhibition. The range of inhibition is plotted with respect to postsynaptic activity. White bars indicate the range of postsynaptic activity recorded, whereas blue bars indicate the frequencies of activity-dependent inhibition (defined as a ≥5% reduction in firing rate). (**b**) Difference in spike-density functions for paired recordings showing instantaneous inhibition with respect to postsynaptic activity and time. (**c**) Example of increased recurrent inhibition during paired mitral-cell stimulation. The black trace shows the control recurrent IPSP and the blue trace shows the recurrent IPSP recorded during stimulation of presynaptic cell. (**d**) Pairs of correlated spikes (blue trace) were not more effective at recruiting granule cell activity than distributed spikes (black trace). (**e**) Activity-dependent range of inhibition between pairs can be modulated by presynaptic firing rate (presynaptic firing rate of 50 Hz in green and 100 Hz in blue). (**f**–**h**) Lower and upper thresholds of the activity-dependent range of inhibition were reduced by increasing presynaptic mitral-cell firing rate while the peak percentage change in activity was increased.

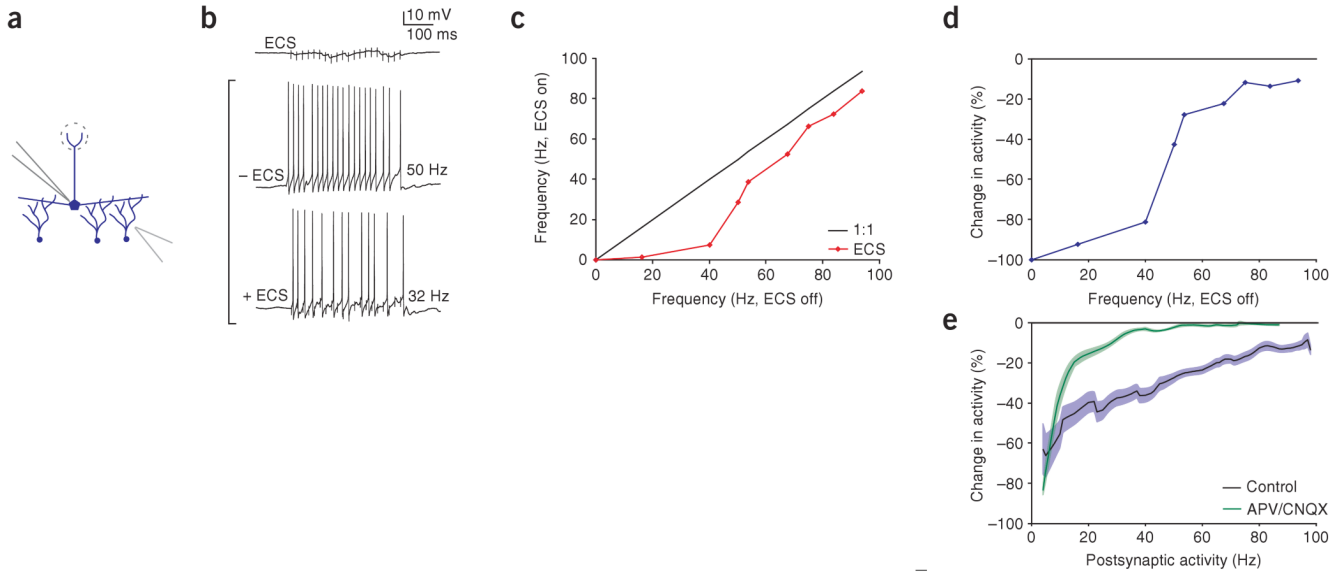

Figure 4.

Lateral inhibition evoked by direct stimulation of granule cells. (**a**) Schematic of experimental configuration. We recorded from a single mitral cell while extracellular stimulation (ECS) was applied in the granule cell layer ~ 200–300 mm away. (**b**) ECS resulted in IPSPs in the mitral cell, and for a given current step ECS reduced the mitral-cell firing rate (50 Hz control firing rate was reduced to 32 Hz when ECS was applied). (c,d) Frequency dependence of inhibition for this example, plotted as the absolute change in frequency (**c**) and as the percent reduction (**d**). (**e**) Aggregate results ($n = 9$ for control in blue and $n = 4$ for APV/CNQX in green) indicated that inhibition evoked via ECS in the granule cell layer showed saturation with increasing postsynaptic frequency, but did not show activity-dependent gating at lower frequencies.

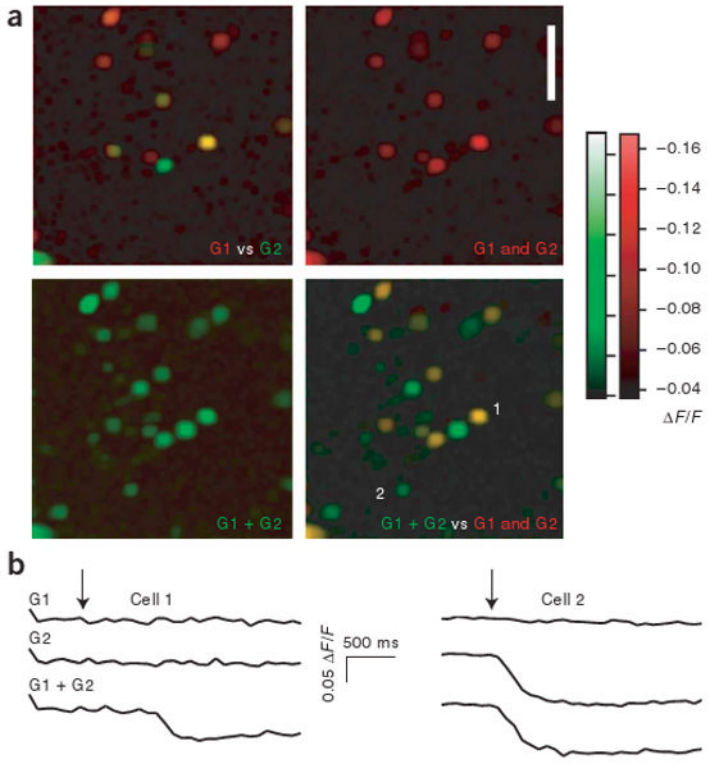

Figure 5.

Overlapping and cooperative activation of granule cells following mitral cell stimulation. (**a**) Imaging of bulk-loaded calcium indicator (fura-2) from a population of granule cell–layer neurons. Images show calcium-induced changes in fluorescence ($\Delta F/F$) from populations of granule cells (images show minimum values for a given pixel across ten trials). The top left image shows the population of granule cells that were activated by stimulation of one glomerulus (G1, red) and a second glomerulus (G2, green). Yellow cells were activated by stimulation of either glomerulus. Top right, merged image in the red channel (G1 and G2). Bottom left, the population of granule cells evoked by simultaneous stimulation of both glomeruli (G1 + G2). Bottom right, the overlay of images from top right and bottom left. This overlay shows the population of granule cells that were activated only by simultaneous stimulation (in green). (**b**) Calcium transients from two cells shown in the images in a. Cells are labeled 1 and 2 in lower right panel of a. Arrows indicate time of stimulation.

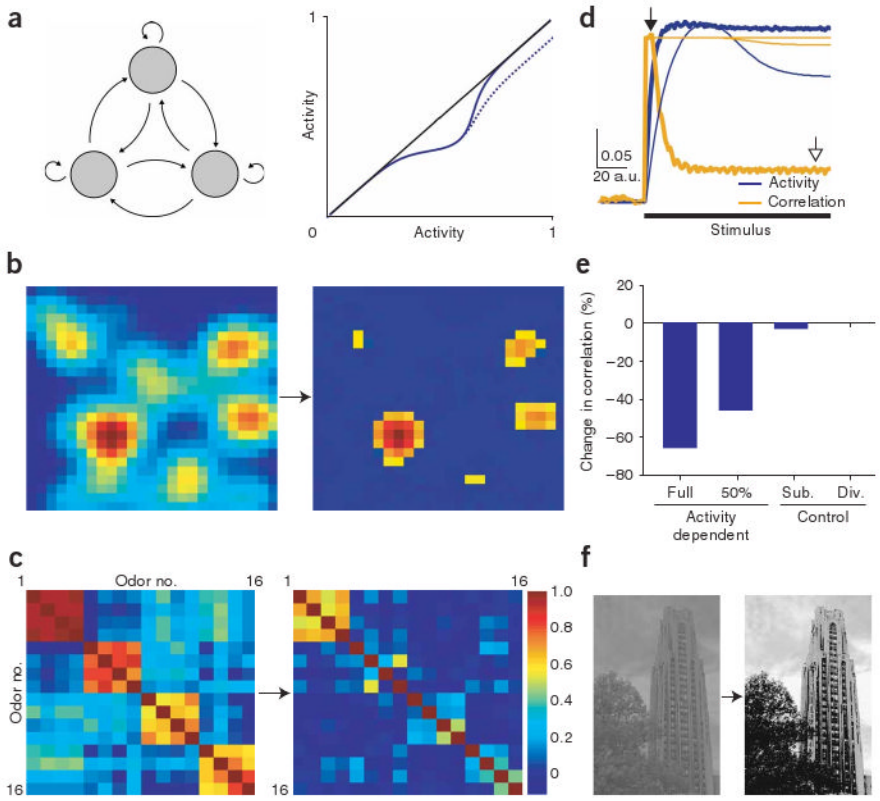

Figure 6.

Activity-dependent lateral inhibition enhances contrast and decorrelates similar patterns of activity. (**a**) Left, schematic of network connectivity of the computational model indicating all-to-all connectivity. Each neuron showed the same type of activity-dependent gating of lateral inhibition as observed in our results (compare right panel of Fig. 6a to Fig. 2d or 1d, activity in Fig. 6a shown in arbitrary units). Two types of activity-dependent inhibition were compared (solid line, full return to baseline activity; dotted line, 50% return to baseline activity). (**b**) Example of a simulated olfactory-response pattern before (left) and after (right, color map rescaled) processing by activity-dependent lateral inhibition. (**c**) Correlation matrix of 16 different olfactory-response patterns of simulated mitral-cell activity before (left) and after (right) activity-dependent lateral inhibition. (**d,e**) Average activity and correlation across all maps for activity-dependent lateral inhibition and other models of inhibition. The initially high correlation (open arrow, 0.33; thick lines, time at which the left panels of **b** and **c** were derived) was substantially decreased by activity-dependent lateral inhibition (closed arrow, 0.11; time at which second panels of **b** and **c** were derived; scale bar, 0.05 correlation units per arbitrary time units), but not for networks with subtractive or divisive inhibition (thin lines). (**f**) Digital image before (left) and after (right) processing with the network model of activity-dependent lateral inhibition.